

# *HST* study of the LMC compact star forming region N83B<sup>\*</sup>

M. Heydari-Malayeri<sup>1</sup>, V. Charmandaris<sup>2</sup>, L. Deharveng<sup>3</sup>, M. R. Rosa<sup>4, \*\*</sup>, D. Schaerer<sup>5</sup>, and H. Zinnecker<sup>6</sup>

<sup>1</sup> DEMIRM, Observatoire de Paris, 61 Avenue de l'Observatoire, F-75014 Paris, France

<sup>2</sup> Cornell University, Astronomy Department, 106 Space Sciences Bldg., Ithaca, NY 14853, USA

<sup>3</sup> Observatoire de Marseille, 2 Place Le Verrier, F-13248 Marseille Cedex 4, France

<sup>4</sup> Space Telescope European Coordinating Facility, European Southern Observatory, Karl-Schwarzschild-Strasse-2, D-85748 Garching bei München, Germany

<sup>5</sup> Observatoire Midi-Pyrénées, 14, Avenue E. Belin, F-31400 Toulouse, France

<sup>6</sup> Astrophysikalisches Institut Potsdam, An der Sternwarte 16, D-14482 Potsdam, Germany

Received 8 January 2001 / Accepted 21 February 2001

**Abstract.** High resolution imaging with the *Hubble Space Telescope* uncovers the so far hidden stellar content and the nebular features of the high excitation compact H II region N83B in the Large Magellanic Cloud (LMC). We discover that the H II region is powered by the most recent massive starburst in the OB association LH 5 and the burst has created about 20 blue stars spread over  $\sim 30''$  on the sky (7.5 pc). Globally N83B displays a turbulent environment typical of newborn massive star formation sites. It contains an impressive ridge, likely created by a shock and a cavity with an estimated age of only  $\sim 30,000$  yr, sculpted in the ionized gas by the powerful winds of massive stars. The observations bring to light two compact H II blobs, N83B-1 and N83B-2, and a small arc-nebula, N83B-3 lying inside the larger H II region. N83B-1, only  $\sim 2''.8$  (0.7 pc) across, is the brightest and most excited part of N83B. It harbors the presumably hottest star of the burst and is also strongly affected by dust with an extinction of  $A_V = 2.5$  mag. The second blob, N83B-2, is even more compact, with a size of only  $\sim 1''$  (0.3 pc). All three features are formed in the border zone between the molecular cloud and the ionized gas possibly in a sequential process triggered by the ionization front of an older H II region. Our *HST* imaging presents an interesting and rare opportunity to observe details in the morphology of the star formation in very small spatial scales in the LMC which are in agreement with the concept of the fractal structure of molecular star forming clouds. A scenario which supports hierarchical massive star formation in the LMC OB association LH 5 is presented.

**Key words.** Stars: early-type – dust, extinction – H II regions – individual objects: N83B – Galaxies: Magellanic Clouds

## 1. Introduction

The giant H II complex N83 (see Fig.1 and Table 1), which lies in the western part of the Large Magellanic Cloud (LMC) symmetrically opposed to the famous 30 Doradus, is a rather scarcely studied star formation site. Henize (1956) identified four ionized gas regions lying in that direction (N83 A, B, C, D). Davies et al. (1976) catalogued the whole gas complex as DEM 22 and found

two more components (DEM 22a and DEM 22d). Radio continuum observations towards N83 (McGee & Newton 1972) revealed the presence of a bright source (MC 16) coinciding with N83A (Caplan & Deharveng 1985). Lucke and Hodge (1970) detected an OB association (LH 5) spanning over 16 square minutes (3600 square pc) around N83. It contains 26 blue stars (Lucke 1974), the brightest of which is Sk-69°30 (Sanduleak 1970), a G5 Ia with a magnitude of  $V = 10.18$  (Massey et al. 2000; Schmidt-Kaler et al. 1999). There is also a very faint early type Wolf-Rayet star of the nitrogen sequence, BAT99-5 (Breysacher et al. 1999 and references therein).

IRAS detected two infrared sources towards N83A and N83B (Israel & Koornneef 1991), and a study of 69 H II regions by Ye (1998), using radio continuum observations obtained at the Molonglo Observatory Synthesis Telescope (MOST) and  $H\alpha$  fluxes, showed

Send offprint requests to: M. Heydari-Malayeri, heydari@obspm.fr

\* Based on observations with the NASA/ESA Hubble Space Telescope obtained at the Space Telescope Science Institute, which is operated by the Association of Universities for Research in Astronomy, Inc., under NASA contract NAS 5-26555.

\*\* Affiliated to the Astrophysics Division, Space Science Department of the European Space Agency.

**Table 1.** Cross identifications for the LMC N83 objects shown in Fig. 1

R.A.(J2000)	Dec.(J2000)	Names	References
04 54 03	-69 12 04	N83A, NGC 1743, SL 87, ESO 56EN21	Bica et al. 1999
04 54 23	-69 11 05	N83B, NGC 1748, IC2 114, LMC-DEM 22c, ESO 56EN24	"
04 54 01	-69 09 25	N83C	"
04 53 56	-69 10 25	DEM22a, NGC 1737, ESO 56EN20	"
04 54 27	-69 09 47	DEM22d	"
04 54 06.26	-69 11 59.6	Sk-69°25	Simbad
04 54 14.26	-69 12 36.4	Sk-69°30, HD 268757, RMC 59	"
04 54 28.05	-69 12 50.1	BAT99-5, Brey-4	Breysacher et al. 1999

that N83A ranks among the four most reddened regions in the LMC where ionized gas is associated with dust. Although N83B was not included in the survey, these findings argued in favor of an important star formation region.

High-resolution neutral atomic hydrogen observations have recently shown a supergiant H I shell in that part of the LMC (Kim et al. 1999). Since the shells are believed to be created by the combined effects of the radiation pressure and the stellar wind of massive stars on the cool interstellar gas, these observations supported the presence of very hot stars towards N83.

Using the 2.2m and 3.6m telescopes of the European Southern Observatory (ESO), Heydari-Malayeri et al. (1990, hereafter Paper I) discovered a compact H II region of  $\sim 5''$  in size towards N83B. This object, which they named N83B-1, turned out to be a member of the so-called high-excitation blobs (HEBs) in the Magellanic Clouds. In contrast to the typical H II regions of the Magellanic Clouds, which are extended structures spanning several minutes of arc on the sky and powered by a large number of hot stars, HEBs are very dense small regions usually  $5''$  to  $10''$  in diameter. At the distance of the Magellanic Clouds this corresponds to sizes of more than 50 pc for normal H II regions and 1 to 3 pc for the blobs. HEBs are in fact associated with young massive stars just leaving their pre-natal molecular cloud (see Heydari-Malayeri et al. 1999c for references). Paper I investigated several physical characteristics of N83B-1, such as the emission spectrum, excitation, extinction, gas density, chemical composition, abundances, etc. Comparison of *JHK* photometry and IRAS spectra indicated the presence of a compact infrared object with apparent dimensions of the order of  $10''$  towards N83B (Israel & Koornneef 1991).

In this paper we use observations obtained with the *Hubble Space Telescope* to study the compact H II region N83B. The higher resolution of *HST* is essential in order to reveal the various emission and dust features of the nebula. Of particular interest is also to study the stellar content of the H II region and our ability to unveil and identify the exciting stars, which up to now have

remained unknown.

## 2. Observations and data reduction

The observations of N83B were performed with the Wide Field Planetary Camera 2 (WFPC2) on board of the *HST* using several broad- and narrow-band filters. The images taken with the broad-band filters (F300W, F467M, F410M, and F547M) were obtained on February 7, 2000 and had as a goal to reveal the details of the stellar content of N83B which was centered on the Planetary Camera (PC). The narrow-band filter images (F487N, F503N and F656N) were obtained on May 21, 2000. In that case the target was centered on the WF2 which has larger pixels and lower noise than the PC CCD and is better suited for detecting faint nebular emission. Exposures were taken at 4 different pointings offset by  $0''.8$  and the exposure times ranged from 10 to 300 sec (see Table 2 for details).

**Table 2.** N83B observations (*HST* GO-8247)

<i>HST</i> filter	Wavelength $\lambda(\text{\AA})$	Exposure time (sec)
F300W (wide-U)	2911	$4 \times 14 = 56$
F410M (Strömgren <i>v</i> )	4090	$4 \times 50 = 200$
F467M (Strömgren <i>b</i> )	4669	$4 \times 35 = 140$
F547M (Strömgren <i>y</i> )	5479	$4 \times 10 = 40$
F487N (H $\beta$ )	4866	$4 \times 260 = 1040$
F502N ([OIII])	5013	$4 \times 300 = 1200$
F656N (H $\alpha$ )	6563	$4 \times 260 = 1040$

The data were processed through the standard *HST* pipeline calibration. Multiple images were co-added using the STSDAS task *imcombine*, while cosmic rays were detected and removed with the STSDAS task *crrej*. Normalized images were then created using the total exposure times for each filter. To extract the positions of the stars, the routine *daofind* was applied to the images by setting the detection threshold to  $5\sigma$  above the local background level. The photometry was performed setting a circular aperture of 3–4 pixels in radius in the *daophot*

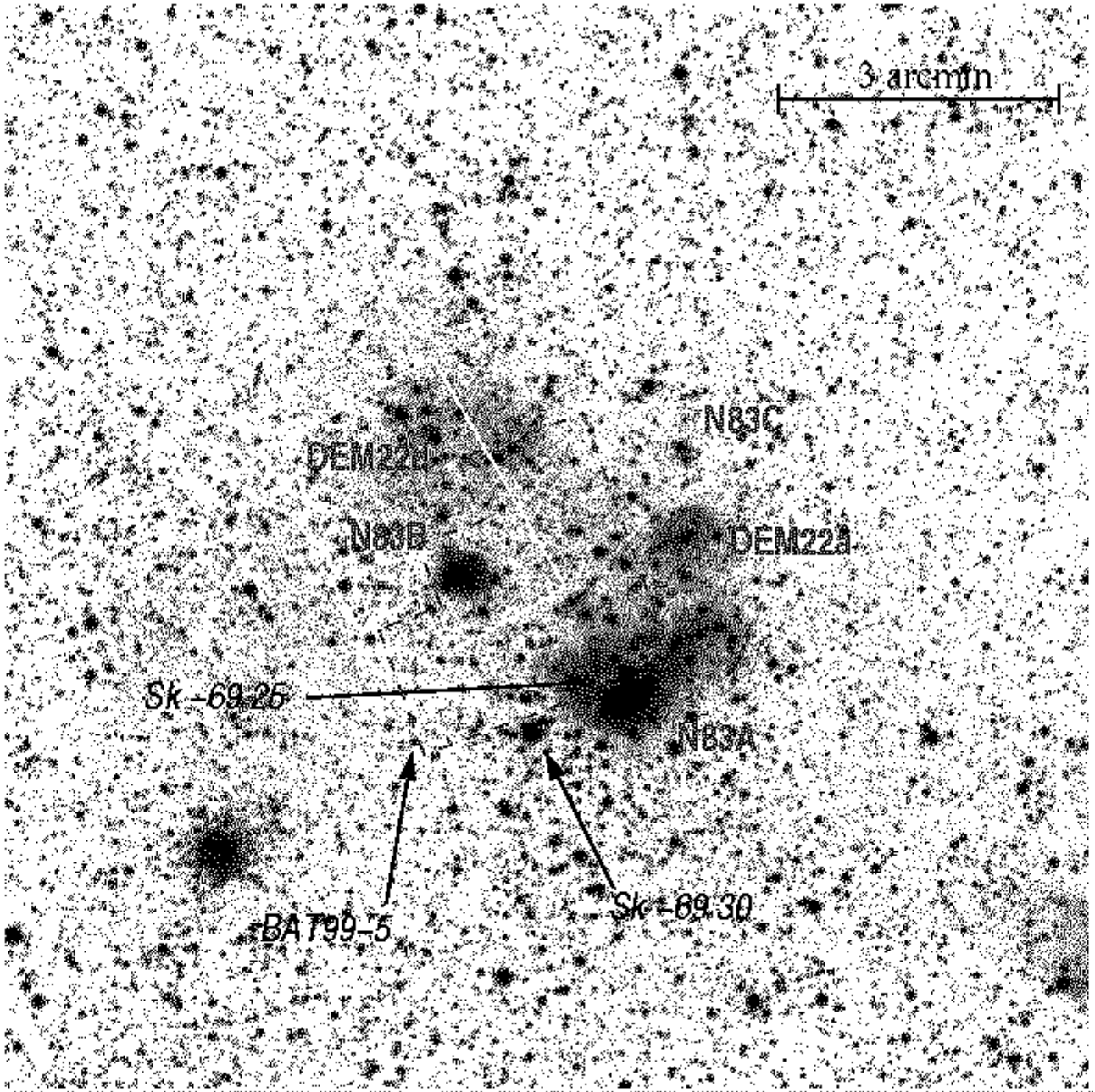


**Fig. 1.** The LMC OB association LH5 with its central giant H II complex N83, as seen on the ESO *R* survey (Simbad server). See Table 1 for cross identifications. The ionized components and three stars of the association are labeled. The marked stars are Sk-69°30, the brightest star of the association, Sk-69°25, the main exciting star of N83A, and BAT99-5, a Wolf-Rayet star (see the text). The WFPC2 footprints are also indicated. The solid line shows the field of view during the *HST* imaging with the nebular filters (21 May 2000) and the dashed line is the one for the stellar filters (7 February 2000). The field center is at:  $\alpha = 04:54:14.48$ ,  $\delta = -69:10:33.7$  (J2000).

package in STSDAS.

A crucial point in our data reduction was the sky subtraction. For most isolated stars the sky level was estimated and subtracted automatically using an annulus of 6–8 pixel width around each star. However this could not be done for several stars located in the central region of N83B due to their crowding. In those cases we

carefully examined the PSF size of each individual star (FWHM  $\sim 2$  pixels, corresponding to  $0''.09$  on the sky) and did an appropriate sky subtraction using the mean of several nearby off-star positions. To convert into a magnitude scale we used zero points in the Vegamag system, that is the system where Vega is set to zero mag in Cousin broad-band filters. The magnitudes measured were corrected for geometrical distortion, finite aperture

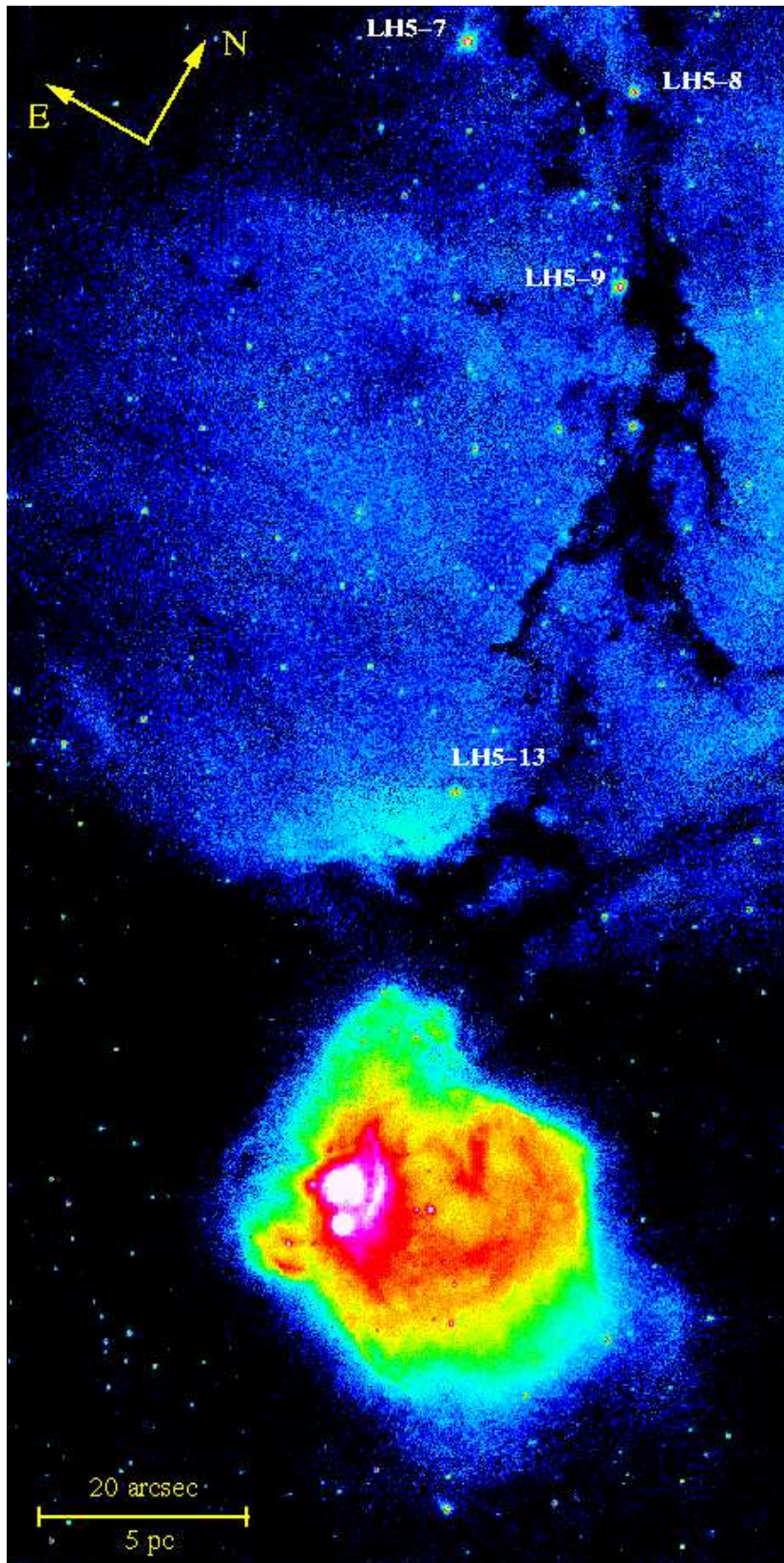


**Fig. 2.** A large view of the LMC compact nebula N83B and its neighboring field imaged with the *HST* camera WFPC2 in the hydrogen recombination line  $H\alpha$  (filter F656N). See Fig. 3 for details of the compact  $HII$  region. The field size is  $\sim 66'' \times 133''$  ( $\sim 17 \text{ pc} \times 33 \text{ pc}$ ) and comprises the images by the CCDs WF2 and WF3. The four bright, labelled stars are known members of the OB association LH5. Downward from top, their  $V$  magnitudes are 13.82, 14.99, 14.16, and 15.16 respectively.





**Fig. 3.** A “true color” composite image of the LMC compact H II region N83B as seen by *HST*/WFPC2, based on images taken with filters  $H\alpha$  (red),  $[O III]$  (green), and  $H\beta$  (blue). The brightest blob is the compact H II region N83B-1 ( $\sim 2''.8$  across, 0.7 pc, surrounding star #29) and the fainter one below it ( $\sim 1''$  in size surrounding star #28) is N83B-2. The small arc-nebula further south, centered on a relatively bright star (#34, see also Fig. 4), is N83B-3. Note also the outstanding shock ridge and the cavity to the west of N83B-1, sculpted in the ionized gas of N83B by the stellar wind of the central bright star (#10), with its shell structure and curl. The field size is  $\sim 63'' \times 63''$  ( $\sim 15$  pc  $\times$  15 pc), and the orientation the same as in Fig. 2.

size (Holtzman et al. 1995), and charge transfer efficiency as recommended by the *HST* Data Handbook. Our broad-band images reveal 179 stars in the WFPC2 field of view. Thirty six (36) of those are confined towards N83B-1 within the area covered the PC. Most of them are also visible in the true-color image (Fig. 3), and can be identified using the finder chart presented in Fig. 4. In Table 3 we summarize the photometry for those stars around N83B-1 (the PC field of view) which are brighter than 19th magnitude in the Strömgren  $y$  filter, as we cannot provide accurate colors for the fainter ones. The photometric errors estimated by *daophot* are smaller than

0.01 mag for the brighter (14–15 mag) stars, while they increase to  $\sim 0.2$  mag for 19 mag stars.

We note that the filter F547M is wider than the standard Strömgren  $y$  filter. To evaluate the presence of any systematic effects in our photometry and color magnitude diagrams due to this difference in the filters, we used the STSDAS package *synphot*. Using synthetic spectra of hot stars, with spectral types similar to those found in H II regions, we estimated the difference due to the *HST* band-passes to be less than 0.002 mag, which is

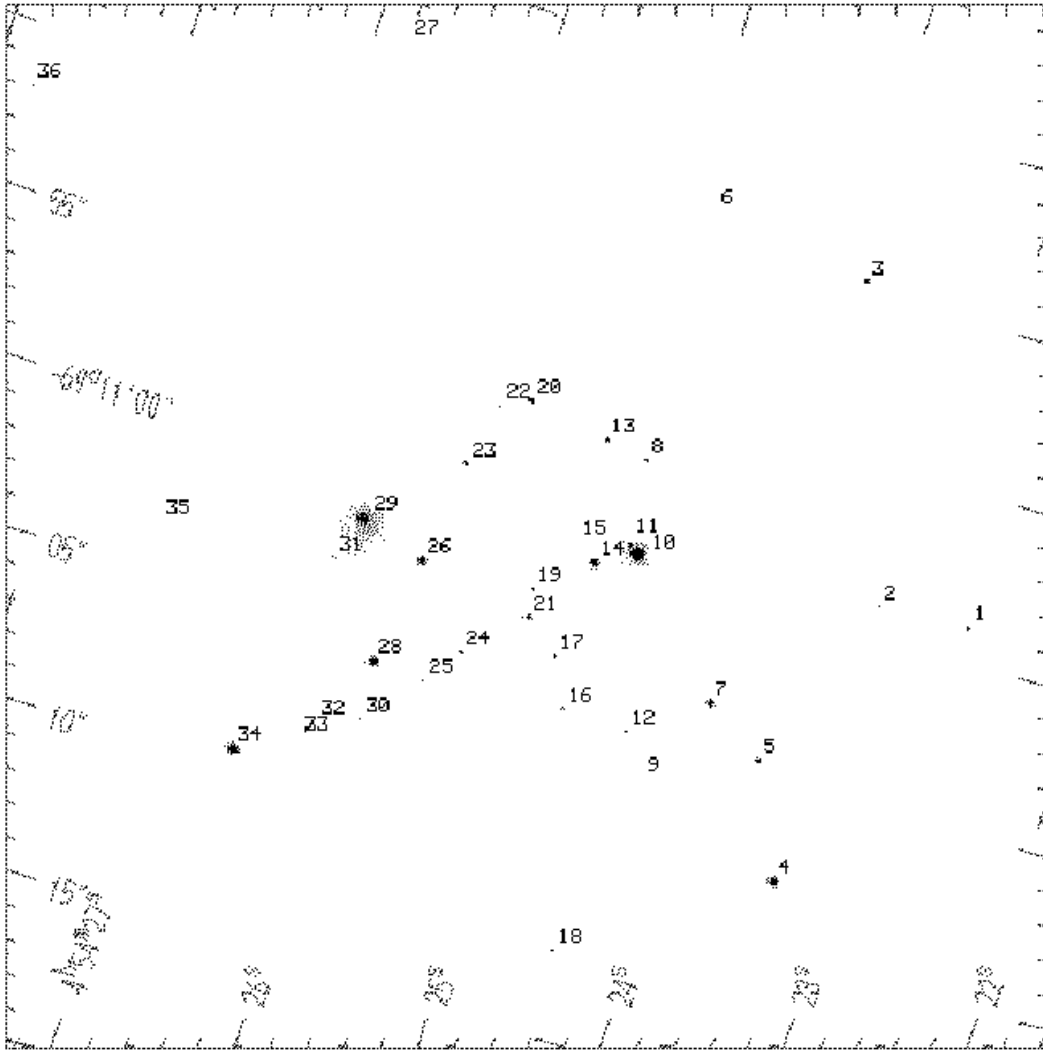


**Fig. 4.** A WFPC2 image of the LMC N83B taken with the Strmgren  $y$  filter (F547M) where the brighter stars are labeled. The photometry of the stellar subsample is presented in Table 3. The field size is  $\sim 32'' \times 32''$  ( $\sim 8 \text{ pc} \times 8 \text{ pc}$ ), and the coordinates are in J2000.

well within the photometric errors.

#34 and presents a relatively bright circular filament or arc to the south.

### 3. Results

#### 3.1. Morphology

A large-scale image of the N83B field in  $H\alpha$  emission obtained with *HST* is shown in Fig. 2, while a close-up view of the  $H\text{II}$  region is presented in Fig. 3. The images for the first time resolve N83B and reveal several interesting nebular and stellar features. The  $H\text{II}$  blob N83B-1, lies in the brightest part of the nebula, and is nearly two times more compact than previously believed ( $\sim 2''.8$  across, 0.7 pc). The images also unveil a previously unknown even smaller  $H\text{II}$  region of  $\sim 1''$  in diameter lying less than  $4''$  south-west of N83B-1. Hereafter we will call it N83B-2. Another interesting ionized region, N83B-3, situated some  $6''.5$  (1.6 pc) south of N83B-1, is centered on star

An outstanding feature, clearly visible in the above figures, is a narrow ridge or partial shell of ionized gas centered on N83B-1 and situated to its west at a projected distance of  $2''.5$  (0.6 pc). This ridge, most probably produced by powerful stellar winds and shocks from the hot stars #29 and #10, indicates a very turbulent environment typical of star forming regions. All these emission features around N83B-1 are found in the eastern part of a larger diffuse nebula  $\sim 30''$  ( $\sim 7.5 \text{ pc}$ ) in diameter, N83B, which displays a shell structure, the northern part of which is abruptly curved to the east. The low brightness at the center of this shell nebula is most likely due to a cavity already created by the brightest star of the region (that is star #10, see Section 3.4).

Further north of N83B the much larger and even more diffuse nebular region DEM 22d is visible (top of Fig. 2). It is crossed by a prominent dark absorption lane extending over more than a minute of arc or 15 pc along the north-northeast direction. This structure is situated in front of the diffuse emission nebula. Even though it is not clearly obvious in the printed version of Fig. 2, inspecting the dark lane in detail, it appears that its borders are enhanced in brightness indicates that it is dense and ionized from outside, probably by the radiation field of the underlying nebula. This structure is somewhat reminiscent of “the gaseous pillars” observed by *HST* in M16.

The filamentary and wind induced structures are best seen in Fig. 5, which presents an un-sharp masking image of N83B in  $H\alpha$  from which large scale structures have been subtracted. In order to remove these brightness variations and enhance the high spatial frequencies, a digital “mask” was created from the  $H\alpha$  image. First the  $H\alpha$  image was convolved by a  $2 \times 2$ -pixel Gaussian, and then the smoothed frame was subtracted from the original  $H\alpha$  image. Interestingly, the inspection of the orientation of these arched filaments suggests the presence of several sources of stellar winds, particularly stars #29, #34, and #10 which are among the brightest blue stars of the cluster.

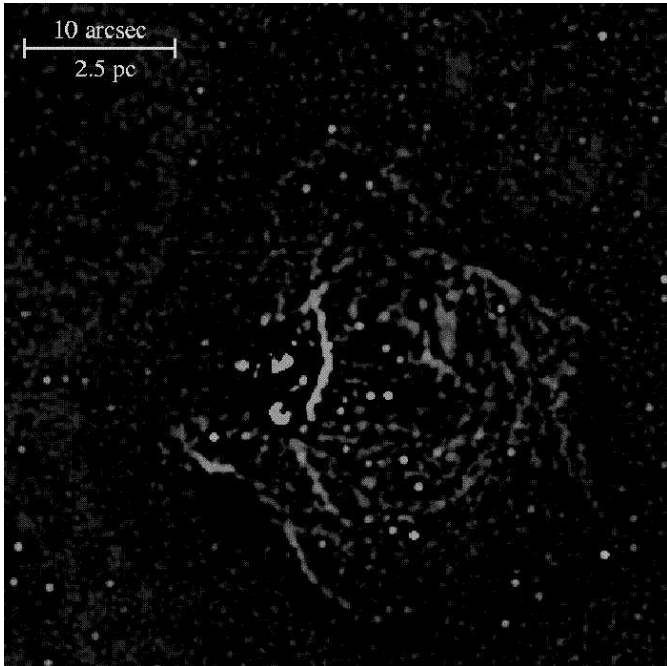


**Fig. 5.** An un-sharp masking image of N83B obtained in  $H\alpha$ , which highlights the filamentary patterns of the nebula (see the text). The field size is  $\sim 45'' \times 45''$  (11 pc  $\times$  11 pc), and the orientation is as in Fig. 4.

### 3.2. Extinction

A map of the  $H\alpha/H\beta$  Balmer decrement is presented in Fig. 6a. It reveals a strong absorption zone coinciding with the  $H\text{ II}$  blob N83B-1, where the ratio reaches values as high as  $\sim 7$ , while its mean value is  $5.10 \pm 0.30$ . Using the interstellar reddening law, these ratios correspond to  $A_V = 2.5$  and 1.6 mag respectively. We note that star #29, the second brightest star in N83B (see Table 3), is situated in the direction of this high extinction region. Another peak with slightly smaller reddening is centered on star #28, located inside the compact blob N83B-2, and reaches a mean  $H\alpha/H\beta$  value of 4.5 corresponding to  $A_V = 1.3$  mag.

Outside those areas the reddening is smaller and becomes almost uniform towards the diffuse component with a mean value of  $\sim 3.7$  which corresponds to  $A_V = 0.7$  mag. For the whole N83B the global Balmer decrement is slightly larger,  $3.85 \pm 0.02$  or  $A_V = 0.8$  mag. This value revises the 3.99 which had been estimated in Paper I. The new  $H\alpha/H\beta$  map was used to accurately correct the  $H\beta$  flux of the  $H\text{ II}$  region for interstellar reddening. The correction was applied to the  $H\beta$  image on a pixel by pixel basis using straightforward mathematical operations. Our interpretation of these results is presented in the following section.

### 3.3. Nebular emission

The  $[\text{O III}]\lambda 5007/H\beta$  intensity map (Fig. 6b) reveals a remarkably extended high-excitation zone where the  $\text{O}^{++}$  ions occupy almost the same volume as  $\text{H}^+$ . However, the most excited area belongs to the compact component N83B-1, where the ratio reaches values as high as  $\sim 6$ , while its mean value is around 4.5. Interestingly, the highest excitation area is at the same time the most reddened part of the nebula (Section 3.2), indicating the association of hot gas with local dust. On the other hand, the diffuse component is significantly less excited with a mean value  $\sim 2$ . The second blob, N83B-2, is of even lower excitation, with  $[\text{O III}]/H\beta \sim 1$ , indicating that its associated exciting star, #28, has a later spectral type than that of star #29, which excites N83B-1, in agreement with the stars’ respective positions in the color-magnitude diagram (Fig. 7). Surprisingly,  $[\text{O III}]/H\beta$  is fairly low ( $\sim 1.5$ ) along the bright narrow ridge. One possibility is that this ridge is an ionization/shock front, seen nearly edge on. This structure is very reminiscent of the “Bright Bar” in the Orion Nebula, a region of enhanced  $H\alpha$  surface brightness with a high  $[\text{N II}]/H\alpha$  ratio (O’Dell 2001, and references therein).

The total  $H\beta$  flux of N83B was derived using the method explained in Section 3.2. The corrected flux is  $F_0(H\beta) = 1.76 \times 10^{-11}$  erg  $\text{cm}^{-2}$   $\text{s}^{-1}$  above  $3\sigma$  level without the stellar contribution and accurate to 3%.

**Table 3.** *HST* Photometry of the brightest stars towards N83B

Star	RA(J2000)	Dec(J2000)	F300W Wide <i>U</i>	F410M Strömgren <i>v</i>	F467M Strömgren <i>b</i>	F547M Strömgren <i>y</i>	Color <i>b - y</i>
1	4:54:22.7	-69:10:59.0	17.57	18.44	18.48	18.61	-0.13
2	4:54:23.3	-69:10:59.2					
3	4:54:23.9	-69:10:49.9	17.07	18.17	18.19	18.17	+0.02
4	4:54:23.4	-69:11:08.2	14.74	16.17	16.35	16.40	-0.05
5	4:54:23.7	-69:11:04.8	16.18	17.62	17.64	17.80	-0.16
6	4:54:24.8	-69:10:49.2					
7	4:54:24.0	-69:11:03.6	15.48	16.99	17.15	17.12	+0.03
8	4:54:24.9	-69:10:57.1	17.56	18.80	18.78	18.84	-0.06
9	4:54:24.3	-69:11:06.5					
10	4:54:24.7	-69:10:59.9	12.56	14.26	14.48	14.57	-0.09
11	4:54:24.7	-69:10:59.8	16.56	17.70	18.13	18.24	-0.11
12	4:54:24.4	-69:11:05.2					
13	4:54:25.0	-69:10:56.9	16.75	18.08	18.22	18.29	-0.07
14	4:54:24.9	-69:11:00.6	15.55	16.93	17.09	17.15	-0.06
15	4:54:25.0	-69:11:00.2					
16	4:54:24.8	-69:11:05.1					
17	4:54:24.9	-69:11:03.7					
18	4:54:24.4	-69:11:12.3					
19	4:54:25.2	-69:11:01.9	17.41	18.77	18.80	18.76	+0.04
20	4:54:25.5	-69:10:56.5	16.29	17.65	17.87	17.78	+0.09
21	4:54:25.2	-69:11:02.8	16.51	17.83	17.87	17.96	-0.09
22	4:54:25.7	-69:10:56.9					
23	4:54:25.8	-69:10:58.9	16.50	17.81	17.98	17.89	+0.09
24	4:54:25.5	-69:11:04.4	17.90	19.00	18.93	19.00	-0.07
25	4:54:25.6	-69:11:05.6					
26	4:54:25.8	-69:11:02.1	15.28	16.63	16.94	16.97	-0.03
27	4:54:26.8	-69:10:47.1					
28	4:54:25.9	-69:11:05.5	14.96	16.51	16.72	16.69	+0.03
29	4:54:26.2	-69:11:01.5	14.66	15.92	16.04	15.85	+0.19
30	4:54:25.9	-69:11:07.3					
31	4:54:26.3	-69:11:02.9					
32	4:54:26.2	-69:11:08.1					
33	4:54:26.2	-69:11:08.2					
34	4:54:26.5	-69:11:09.4	14.11	15.52	15.80	15.86	-0.06
35	4:54:27.3	-69:11:03.4					
36	4:54:28.8	-69:10:51.9					

Assuming that the H II region is ionization-bounded, the corresponding Lyman continuum flux of the region is  $N_L = 1.37 \times 10^{49}$  photons  $s^{-1}$ . A single main sequence star of type O6.5 or O7 or several massive stars of later types can account for this ionizing UV flux (Vacca et al. 1996, Schaerer & de Koter 1997). However, these are apparently underestimates since the H II region is more likely to be density-bounded, as the west side of it, i. e. the diffuse shell nebula, appears to be torn open towards the interstellar medium.

### 3.4. Stellar content

The stars of the region imaged by HST have magnitudes ranging from  $y = 14.57$  to  $\sim 22$ . Using a magnitude cutoff of  $y = 19$ , we construct a color-magnitude (C-M) diagram of  $y$  versus  $b - y$  (Fig. 7) in which we have also

added all the background stars around N83B visible in the whole field of WFPC2. The C-M diagram displays a rather well-defined main sequence for the N83B cluster in the interval  $14.56 \leq y \leq 19.00$  centered on colors  $b - y = -0.04$ , or  $v - b = -0.13$ . The colors and absolute magnitudes (see below) are typical of massive OB stars (Relyea & Kurucz 1978, Conti et al. 1986, Vacca et al. 1996). There is no evidence for stars evolved off the main sequence in N83B. We note that star #29 is offset red-wards ( $b - y = +0.19$ ) in the C-M diagram. However, since it lies in the most heavily obscured area of the N83B-1 blob, it is quite probable that its color is reddened due to extinction by dust (see Section 3.2), and star #29 may be in fact intrinsically blue and one of the main exciting stars of the region. Similar reasoning could explain the rather red colors of two more stars, #23 which is situated on the bright ridge and #20 found just



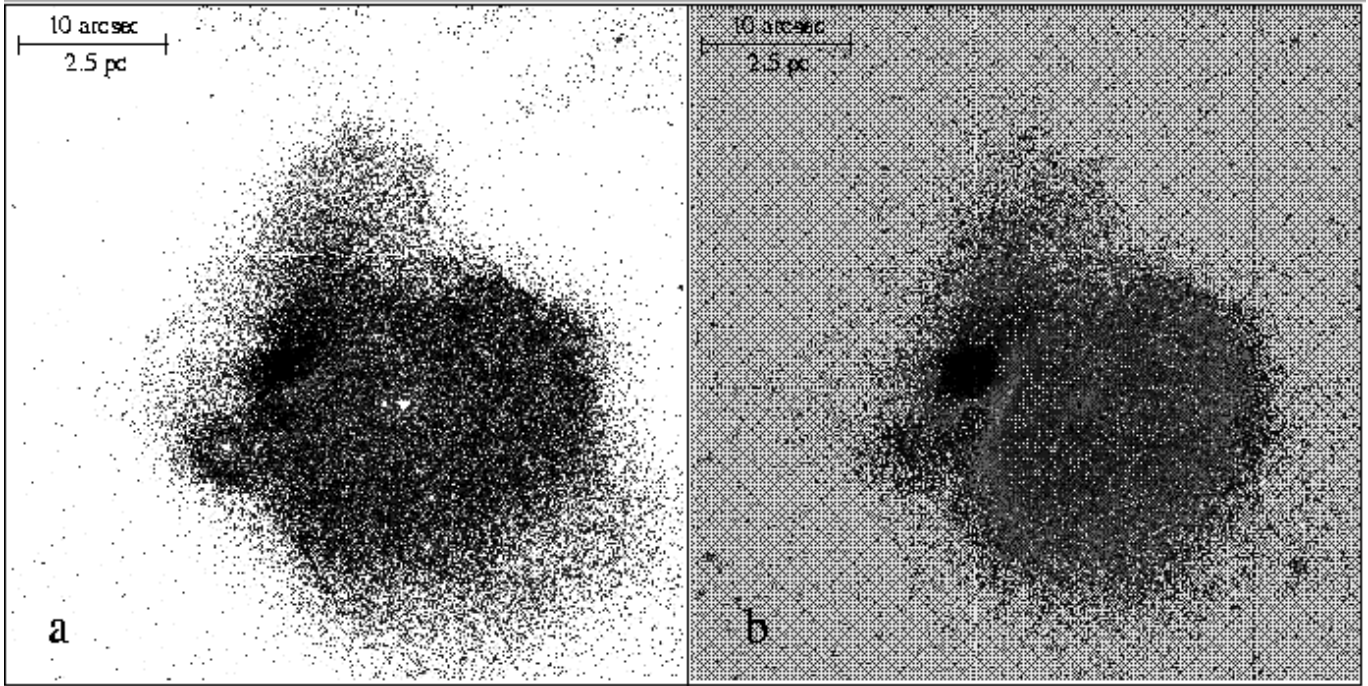


**Fig. 6.** Line intensity ratios for the LMC compact nebula N83B. Darker colors correspond to higher ratio values. The field of view and orientation are identical to Fig. 5. The white spots are stars and can be identified using Fig. 4. **a)** Balmer decrement  $H\alpha/H\beta$ . Its mean value over the diffuse component is  $\sim 3.7$  ( $A_V = 0.7$  mag), while the ratio goes up to  $\sim 7$  ( $A_V = 2.5$  mag) towards the compact blob N83B-1. **b)** The  $[O\ III]\lambda 5007/H\beta$  ratio, where the highest values, towards N83B-1, reach  $\sim 6$ .

to the north side of the ridge.

The brightest star observed is #10 situated towards the center of the diffuse shell nebula. It has a faint visual companion, #11, lying just  $0''.3$  to its east. The second brightest star is #94 which is a field star apparently associated with the main ionized gas component N83A; its J2000 coordinates are:  $\alpha = 4:54:15.6$ ,  $\delta = -69:12:14.9$ . Following in brightness are stars #29 and #34 of N83B, the latter of which ionizes the nebula N83B-3. Another noteworthy star is #28 which lies inside the small nebular blob N83B-2. It should be a massive star responsible for the ionization of the compact nebula. Stars #34 and #28 are less reddened than star #29 in agreement with the fact that the extinction of their associated nebulae, estimated from the Balmer decrement, is smaller than that of N83B-1.

One could try to estimate the luminosities of the brightest stars of the cluster (#10 and #29), although in the absence of spectroscopic data this would not be accurate. In the case of star #10, using an extinction of  $A_V = 0.7$  mag corresponding to the mean value for the associated nebula (Section 3.2), and a distance modulus  $m - M = 18.5$  (e.g. Kovács 2000 and references therein), we find a visual absolute magnitude  $M_V = -4.63$ . If the star is on the main sequence, according to the calibration of Vacca et al. (1996) for Galactic stars, it would be an O8V. The corresponding luminosity and mass would

be  $\log L = 5.235 L_\odot$  and  $M = 30 M_\odot$ . The reddening correction for star #29 is more important since the star is embedded in a region where the extinction reaches a value of  $A_V = 2.5$  mag. Correcting for the reddening the absolute magnitude of the star is estimated as  $M_V \sim -5$ , which corresponds to a main sequence O6 star with a ZAMS mass of  $45 M_\odot$  (Vacca et al. 1996).

Apart from the main sequence, the C-M diagram shows several stellar populations with a variety of red colors. These should be a mix of stars in different stages of evolution affected by the interstellar dust along the line of sight. Disentangling those populations is not an easy task and doing so using just the present data would be rather speculative.

#### 4. Discussion

It is interesting to speculate about the physical conditions that led to the formation of the two adjacent ionized blobs (N83B-1 and N83B-2) inside the larger N83B and understand why they have different sizes. Of course the size depends on the mass or temperature of the exciting stars, but also on the density of the molecular clumps. On the other hand, the mass of the exciting stars themselves might depend on the clump density in which they formed. So, was the initial density of the molecular clumps the main factor, denser clumps formed more massive stars,

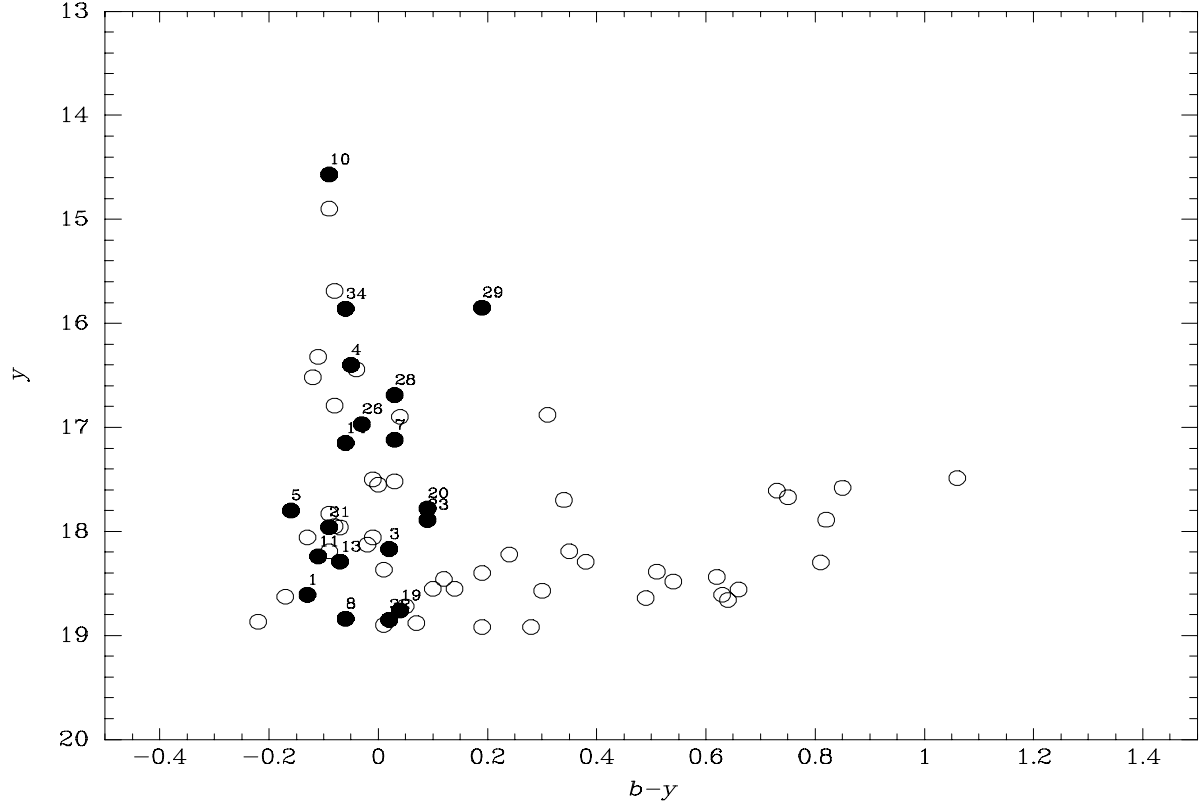


**Fig. 7.** Color-magnitude diagram of the brightest stars (lower cutoff at  $y = 19$  mag) observed towards the H II region N83B based on WFPC2 imaging with the Strömgren filters  $b$  (F467M) and  $y$  (F547M). The magnitudes are not corrected for the reddening. A solid dot indicates a stars lying in the PC field (i.e. the area surrounding N83B), while an open circle marks a star found in the three WF CCDs.

or were there random factors at work in a very turbulent environment? We cannot provide a definite answer to all these questions, but we will try to probe some of the issues by placing these objects into the global star formation history of the region. To do so let us examine the N83 region in more detail.

The N83 ionized gas complex occupies the central part of the LMC OB association LH5 (Lucke & Hodge 1970) and is dominated by the bright and large H II region N83A (Fig. 1). The main exciting star of N83A, Sk-69°25 (Sanduleak 1970), is an O6 V(f) type with  $V = 12.28$ ,  $B - V = -0.14$ , and  $U - B = -0.97$  mag (Massey et al. 2000; Schmidt-Kaler et al. 1999). An age of 2.24 Myr and a ZAMS mass of  $64 M_{\odot}$  are estimated for this star (Massey et al. 2000). Unfortunately little is known about the stellar content and detailed physical properties of N83A. We do know however that it is associated with a large quantity of dust, as shown by the IRAS observations or by its strong extinction (Caplan & Deharveng 1986, Ye 1998). An  $H\alpha/H\beta$  ratio of 3.77 derived by these authors for the whole N83A indicates an interstellar extinction of  $A_V = 0.8$  mag.

On the other hand, N83B which lies at  $\sim 2'$  ( $\sim 30$  pc) north-east of N83A (Fig. 1), probably represents the most recent massive starburst in the giant H II complex N83 and the OB association LH5. The young age is inferred from the fact that the burst is associated with a compact high-excitation H II blob, N83B-1, which is strongly affected by local dust. The extreme youth of N83B is corroborated by the results of Israel & Koornneef (1991) who conducted a  $JHK$  survey of the LMC H II regions and compared it with the IRAS observations. In the case of N83B, they detected a compact source of less than  $10''$  in size at both near-IR and IRAS wavelengths, whereas no compact source was found towards N83A. An inspection of their Table 3 shows that all very young star formation regions are associated with compact IR sources, as is particularly the case for other Magellanic H II blobs, such as N159-5, N81, and N88A (Heydari-Malayeri et al. 1999 a,b,c), as well as for many Galactic H II regions.

The *HST* observations reveal those, so far hidden, components of N83B and bring to light a starburst made of dozens of newborn stars. As discussed earlier, the star cluster consists of a well-defined main sequence population with 19 members ranging in magnitude from

$y = 14.57$  to  $19.00$  spreading over  $56 \text{ pc}^2$ . They are all associated with the H II region and many of them participate in its ionization. Our observations also imply that the true number of massive stars in the LMC is underestimated, since a large number of them should be hidden in similarly unresolved small clusters. Based on the number of detected stars over the area imaged by HST we estimate a surface density of  $0.34 \text{ stars pc}^{-2}$  for massive stars in N83B, which is quite high, a factor of  $\sim 50$  higher than that for LH5 (Lucke 1974), and even a factor of 17 higher than the mean density derived for a sample of five OB associations in the Magellanic Clouds (Massey et al. 1995, Hunter 1995). Though the total number of massive stars is not well determined, even if we reduce them to 10 the corresponding density is  $0.18 \text{ stars pc}^{-2}$  which is still  $\sim 10$  time larger than that of the Magellanic Clouds OB associations. The star density in the N83B-1 area is in fact higher than that, since we are quite certain that at least stars #10, #28, #29, and #34 are all massive and hot occupying an area of only  $7 \text{ pc}^2$ . This yields a density of  $0.57 \text{ stars pc}^{-2}$  which is interestingly just  $\sim 3$  times smaller than that of R136 (Hunter 1995). One should keep in mind though that the above comparisons may not reveal the whole picture as they may be affected by the small-number statistics due to the size of our regions and also by the uncertainties on the number of candidate massive stars. On the other hand, a recent study by Parker et al. (2001) shows that field stars significantly contaminate the massive star population of the LMC OB associations, and hence the corresponding initial mass functions. Consequently, this tends to aggravate the discrepancy in the estimated stellar densities.

Furthermore, our imaging clearly shows the structure of the two compact H II blobs, N83B-1 and N83B-2, and the small arc-nebula, N83B-3, bathing in N83B. The first one represents the brightest and the most excited region of N83B. Its exciting star, #29, is presumably the most massive and hottest star of the burst, since it is responsible for the particularly high excitation measured from the strength of the doubly ionized oxygen line. As for the smaller blob N83B-2, its ionizing source (#28) is expected to be a late type O or an early B, since the nebular  $[\text{O III}]/\text{H}\beta$  ratio is not large. The same should be true for #34, the exciting star of N83B-3. The relatively high brightness of the arc south of this nebula suggests the presence of high density material also in that direction.

The blob N83B-1 is likely the most obscured part of the N83 complex with  $A_V \sim 2.5 \text{ mag}$ . It is probably the optical counterpart of the compact IR source detected by Israel & Koornneeff (1991). While dust may be mixed with ionized gas, such a large extinction implies the presence of dust also outside the nebula, since the Balmer decrement due to absorption by internal dust becomes saturated at a ratio of 4.3 (for  $R = A_V/E(B - V) = 3.1$ ) or  $A_V = 1.1 \text{ mag}$ . Note also that the H II region's

mean  $\text{H}\alpha/\text{H}\beta$  ratio of 3.85 is higher than the value of 3.77 obtained for N83A (Caplan & Deharveng 1986, Ye 1998). An extinction of  $A_V = 0.5 \text{ mag}$  derived for Sk-69°25 from its photometry and spectral type indicates that the main exciting star of N83A is not situated in the most reddened part of the H II region, contrarily to what is the case for #29, the exciting star of N83B-1.

A rather noteworthy point is the presence of the three H II region N83B-1, 2, and 3 at the same side of N83B. This alignment need not be by chance, but probably due to the presence of the adjacent molecular cloud. The particularly high extinction of N83B-1 can be explained by the presence of dust associated with the molecular cloud very probably located east of N83B-1 and south of N83B-3. In fact the brightest area of the nebula, the blob N83B-1, is expected to lie near the intersection zone between the ionized gas and the molecular cloud. Two different models can be proposed to explain the observed morphology. According to the first one, N83B-1 and the shell nebula may be two parts of the same H II region. In that case the H II region is probably ionization-bounded towards N83B-1, while ionized gas is pouring out into the interstellar medium mainly via the diffuse component, as predicted by the champagne model (Tenorio-Tagle 1979, Bodenheimer et al. 1979). Alternatively, we may be watching four separate H II regions: N83B-1 which is still embedded in the molecular cloud, N82B-2, N83B-3, and the shell nebula, which should be a relatively evolved H II region.

In the framework of the latter model, which we favor, N83B-1 is expected to be younger than the diffuse shell nebula, because it is compact, denser, and still embedded in the molecular cloud. This leads to the conjecture that the exciting stars of N83B-1 and N83B-2, i.e. #29 and #28, may have been triggered by the eastward expansion of the shell nebula according to the sequential star formation model (Elmegreen & Lada 1977). There are many cases in the literature for which this mechanism has been put forward to explain the observations, in particular that of the SMC H II region N88A (Heydari-Malayeri et al. 1999b).

A conspicuous feature of N83B uncovered by the *HST* images is the cavity carved in the diffuse nebula by the strong wind of the central star #10 which has a particularly strong ultraviolet radiation (Table 3). We try here to estimate an age for the cavity. Assuming a typical mass loss rate of  $6 \times 10^{-5} M_{\odot} \text{ yr}^{-1}$  for the presumed central O star, a conservative wind velocity of  $1000 \text{ km s}^{-1}$ , a gas density of  $100 \text{ cm}^{-3}$ , and an observed radius of  $2.5 \text{ pc}$ , we find a lifetime of  $37,000 \text{ yr}$  from the classical equations governing the interaction of the stellar wind and the interstellar medium (Weaver et al. 1977, Dyson 1978). Should the wind velocity be higher,  $2000 \text{ km s}^{-1}$ , the corresponding age will be  $23,000 \text{ yr}$ . In the same way, we can calculate the age of the sharp emission ridge with the

assumption that it is created by star #29. Using the same mass loss rate as the one adopted for #10, a wind velocity of  $1000 \text{ km s}^{-1}$ , a gas density of  $1000 \text{ cm}^{-3}$  (Paper I), and a projected radius of 0.6 pc, we derive an age of 7400 yr for the bright ridge. It is also possible that the ridge in fact results from the interaction of the winds of both stars #29 and #10. Consequently, its true age may be larger if the wind of star #10 significantly decelerates the westward advance of the ridge and/or if its assumed radius is actually underestimated due to projection effects.

These new *HST* data combined with large-scale, low-resolution observations obtained with ground-based telescopes provide new evidence in favor of hierarchical star formation (Elmegreen & Efremov 1996, Elmegreen 2000) in this region. According to this model, large-scale star-forming regions have a fractal architecture, in the sense that the cloud structures appear self-similar over a wide range of scales. The gas structures range from superclouds ( $\sim 10^7 M_\odot$ ) in which star complexes form, to giant molecular clouds ( $10^3$  to  $10^6 M_\odot$ ) in which clusters and OB associations form, to small molecular cores ( $< 10^3 M_\odot$ ) in which individual and multiple stars form (Elmegreen & Efremov 1996). A recent study by Elmegreen (2000) of the age difference versus size has yielded an interesting correlation for 244 LMC clusters with size and age ranges  $\sim 0.1$ –1000 pc and 10–100 Myr, respectively. It turns out that the timescale for coherent star formation in a region is always about one turbulent crossing time (defined as half-size divided by the Gaussian dispersion in internal velocity), scaling approximately with square root of size. This implies that small regions should evolve faster than large regions: inside the larger regions, numerous smaller regions form and dissolve many times over a relatively long period.

This scenario seems very attractive for the OB association LH5 and the H II complex N83. In other words the *HST* observations provide a rare case in which by penetrating into very small spatial scales in the LMC we discover a fractal star-forming region. The OB association LH5, which spreads over an area of 16 square minutes (3600 square pc), harbors tens of bright, blue and red stars as well as several H II regions. None of the brightest stars lie in the *HST* field of view, except the ones indicated in Fig. 1. The brightest star of the association, Sk-69°30 (Sanduleak 1970), is in fact an evolved supergiant of type G5 Ia (Massey et al. 2000) with  $V = 10.18$  mag (Schmidt-Kaler et al. 1999). The association contains also a Wolf-Rayet star of type WN2, called BAT99-5 (Conti & Massey 1989; Breysacher et al. 1999), which naturally comes from the evolution of a massive O type progenitor. Using photometry and spectroscopy to construct the HR diagram and by fitting isochrones, Massey et al. (2000) estimate an age of 1.26 to 2.24 Myr for the brightest main sequence O type stars of the association, while they derive an age of 6.46 Myr for the supergiant Sk-69°30 (Fig. 1). On the other hand,

almost all of the known O type stars of LH5 either lie outside the H II regions, or are associated with diffuse, low-density ionized gas, implying that these stars have had enough time to fully or partially dissipate their H II regions. All these facts support a scenario of continuous massive star formation with an age spread in the OB association LH5, in agreement with a timescale of  $\sim 9$  Myr estimated from Elmegreen’s (2000) hierarchical scaling law.

At a lower level, N83A, the largest H II region of the association, extends over  $\sim 2'$  or  $\sim 30$  pc. Let us assume that the H II region traces the size of the molecular clump which formed the stars in N83A. One may argue that this is not justified if the associated burst is tightly packed and the hot gas expands fast. However, the diffuse structure of N83A which shows no conspicuous brightness peak supports the assumption. Using the same law, a timescale of  $\sim 6$  Myr is therefore expected for the star formation in N83A, and this is in agreement with the above-mentioned age estimate of 2.24 Myr for Sk-69°25, the main exciting star of N83A.

The brighter and more compact H II region N83B has a diameter of  $\sim 30''$  or 7.5 pc, and the uncovered main sequence blue stars extend over almost the same area. Therefore the hierarchical scaling law predicts a younger age of  $\sim 3$  Myr for this region which is consistent with the evidence we presented in this paper suggesting that N83B is in fact younger than N83A.

Going down towards even smaller scales, the presence of the two blobs N83B-1 and N83B-2 and the arc-nebula inside N83B advocates the idea of a fractal structure in the molecular cloud which gave rise to star formation in this part of the LMC. This obviously presumes that even the sequential star formation needs a pre-existing gas concentration, since it only provokes the collapse of the gas and will be inoperative in its absence. The corresponding timescale for N83B-1, as predicted by the hierarchical model, is  $\sim 1$  Myr and follows our scenario in which we have argued that N83B-1 is the youngest and most massive product of star formation in this region.

If the described size-age relation is valid at even lower spatial scales, the H II region N83B-2 should be younger than N83B-1, as its size is smaller. However, at this stage we have no solid evidence on the age of N83B-2 which would corroborate this assertion. As discussed earlier, the  $[\text{O III}]/\text{H}\beta$  ratios indicate that the exciting star of N83B-2 (#28) may actually be less massive than the one inside N83B-1 (#29). Should this be the case, this does not contradict the scenario of fractal star forming structures, as it is possible that in that location the physical conditions (e.g. lack of a large molecular cloud) were not favorable for the formation of a more massive star. Some of these uncertainties may be resolved in the future if spectra of these stars are obtained and accurate ages are estimated.

## 5. Conclusions

Based on the new *HST* observations of N83B described in the paper, we conclude the following:

1) The so-called high excitation blob N83B is resolved into two extremely compact regions N83B-1 and N83B-2. Together with the arc-nebula N83B-3, all three are located in the eastern edge of N83B and their origin appear to be the result of triggered/sequential star formation.

2) A large number of candidate massive stars is revealed making the stellar surface density of the region several times larger than what is typically found in other the OB associations of the Magellanic Clouds.

3) Taking into account the observations ranging from large scales (of order 100 pc, see Fig. 1) to small scales (of order 1 pc, Fig. 3) seems to indicate that indeed the age of a star formation region scales with the square root of its size (1 Myr for 1 pc). The underlying reason for this scaling relation (“star formation law”) could be sought in the fact that the mean gas density of a star forming region is inversely proportional to its linear dimension such that the mean gas column density is constant for all scales. Since the dynamical timescale is inversely proportional to the square root of the mean density (1 Myr for  $10^3 \text{ cm}^{-3}$ ), the dynamical time would scale with the square root of the size.

*Acknowledgements.* The authors are grateful to the referee Dr. Joel Wm. Parker (Southwest Research Institute) whose useful comments contributed to improve the paper. We are also indebted to Dr. Bruce Elmegreen (IBM Research Division) for reading the manuscript and discussion. VC would like to acknowledge the financial support for this work provided by NASA through grant number GO-8247 from the STScI, which is operated by the Association of Universities for Research in Astronomy, Inc., under NASA contract 26555.

## References

- Bica E.L.D., Schmitt H. R., Dutra C.M., Oliveira H.L., 1999, *AJ* 117, 238
- Bodenheimer P., Tenorio-Tagle G., Yorke H.W., 1979, *ApJ* 233, 85
- Breysacher J., Azzopardi M., Testor G., 1999 *AASS* 137, 117
- Caplan J., Deharveng L., 1985, *A&ASS* 62, 63
- Caplan J., Deharveng L., 1986, *A&A* 155, 297
- Conti P.S., Garmany D., Massey P., 1986, *AJ* 92, 48
- Conti P.S., Massey P., 1989, *ApJ* 337, 251
- Davies, R.D. Elliott K.H., Meaburn J., 1976, *MNRAS* 81, 89
- de Koter A., Heap S.R., Hubney I., 1997, *ApJ* 477, 792
- Dyson J.E., 1978, *A&A* 62, 269
- Elmegreen B.G., 2000, *ApJ* 530, 277
- Elmegreen B.G., Efremov Y.N., 1996, *ApJ* 466, 802
- Elmegreen B.G., Lada C.J., 1977, *ApJ* 214, 725
- Henize K.G., 1956, *ApJS* 2, 315
- Heydari-Malayeri M., Van Drom E., Leisy P., 1990, *A&A* 240, 481 (Paper I)
- Heydari-Malayeri M. Rosa M.R., Zinnecker H., Deharveng L., Charmandaris V., 1999a, *A&A* 344, 848
- Heydari-Malayeri M., Charmandaris V., Deharveng L., Rosa M.R., Zinnecker H., 1999b, *A&A* 347, 841
- Heydari-Malayeri M., Rosa M.R., Charmandaris V., Deharveng L., Zinnecker H., 1999c, *A&A* 352, 665
- Holtzman J., Hester J.J, Casertano S., et al., 1995, *PASP* 107, 156
- Hunter D.A., 1995, *Rev. Mex. A.A.* 3, 1
- Israel F. P., Koornneef J., 1991, *A&A* 248, 404
- Kim S., Dopita M. A., Staveley-Smith L., Bessell M.S., 1999, *AJ* 118, 2797
- Kovács G., 2000, *A&A* 363, L1
- Lucke P.B., 1974, *ApJS* 28, 73
- Lucke B.P., Hodge P.W., 1970, *AJ* 75, 171
- Massey P., Johnson K.E., DeGioia-Eastwood K., 1995, *ApJ* 454, 151
- Massey P., Waterhouse E., DeGioia-Eastwood K., 2000, *AJ* 119, 2214
- McGee R.X., Newton L.M., 1972, *Aust. J. Phys.* 25, 619
- O’Dell C.R., 2001, *PASP* 113, 29
- Parker J. Wm., Zaritsky D., Stecher T.P., Harris J., Massey P., 2001, *AJ* 121, 891
- Relyea L.J., Kurucz R.L., 1978, *ApJS* 37, 45
- Sanduleak N., 1970, *Cerro Tololo Inter-American Obs., Contribution No 89*
- Schaerer D., de Koter A., 1997, *A&A* 322, 598
- Schmidt-Kaler Th., Gochermann J., Oestreicher M.O., et al., 1999, *MNRAS* 306, 279
- Tenorio-Tagle G., 1979, *A&A* 71, 79
- Vacca W.D., Garmany C.D., Shull J.M., 1996, *ApJ* 460, 914
- Weaver R., McCray R., Castor J., et al., 1977, *ApJ* 218, 377
- Ye T., 1998, *MNRAS* 294, 422